

Solid-Density Ion Temperature from Redshifted and Double-Peaked Stark Line Shapes

B. F. Kraus^{1,2,*}, Lan Gao², K. W. Hill², M. Bitter², P. C. Efthimion², T. A. Gomez³, A. Moreau⁴,
R. Hollinger⁴, Shoujun Wang⁴, Huanyu Song⁴, J. J. Rocca^{4,5} and R. C. Mancini⁶

¹*Department of Astrophysical Sciences, Princeton University, Princeton, New Jersey 08544, USA*

²*Princeton Plasma Physics Laboratory, Princeton University, Princeton, New Jersey 08543, USA*

³*Sandia National Laboratory, Albuquerque, New Mexico 87123, USA*

⁴*Electrical and Computer Engineering Department, Colorado State University, Fort Collins, Colorado 80523, USA*

⁵*Physics Department, Colorado State University, Fort Collins, Colorado 80523, USA*

⁶*Department of Physics, University of Nevada, Reno, Nevada 89557, USA*



(Received 9 April 2021; revised 27 August 2021; accepted 1 October 2021; published 12 November 2021)

He β spectral line shapes are important for diagnosing temperature and density in many dense plasmas. This work presents He β line shapes measured with high spectral resolution from solid-density plasmas with minimized gradients. The line shapes show hallmark features of Stark broadening, including quantifiable redshifts and double-peaked structure with a significant dip between the peaks; these features are compared to models through a Markov chain Monte Carlo framework. Line shape theory using the dipole approximation can fit the width and peak separation of measured line shapes, but it cannot resolve an ambiguity between electron density n_e and ion temperature T_i , since both parameters influence the strength of quasistatic ion microfields. Here a line shape model employing a full Coulomb interaction for the electron broadening computes self-consistent line widths *and redshifts* through the monopole term; redshifts have different dependence on plasma parameters and thus resolve the $n_e - T_i$ ambiguity. The measured line shapes indicate densities that are 80–100% of solid, identifying a regime of highly ionized but well-tamped plasma. This analysis also provides the first strong evidence that dense ions and electrons are not in thermal equilibrium, despite equilibration times much shorter than the duration of x-ray emission; cooler ions may arise from nonclassical thermalization rates or anomalous energy transport. The experimental platform and diagnostic technique constitute a promising new approach for studying ion-electron equilibration in dense plasmas.

DOI: 10.1103/PhysRevLett.127.205001

Spectral transition lines emitted from plasmas are shifted and widened by the Stark effect, especially in dense plasmas where charged particles enhance electric microfields at the emitting ion [1,2]. Modeling these Stark line shapes and using them to diagnose plasma conditions have been a longstanding goal of white dwarf photosphere studies [3–5], general astrophysics [6,7], and high-energy-density science [8–11]. Several line complexes, particularly the He-like $n = 3 \rightarrow 1$ (He β) transition, have received special attention due to strong Stark broadening and weak opacity effects; He β and its satellites have been used for decades to estimate plasma temperature and density [12], especially in inertial confinement fusion [13–15]. However, both theoretical and experimental obstacles have persisted. Making line shape calculations tractable usually introduces approximations that have been difficult to benchmark; numerous and competing improvements to models have arisen to explain novel measurements [16–20], but these can be limited in scope, buffered by empirical assumptions, and at times heuristic in nature. Line shape measurements, on the other hand, often come from inhomogeneous plasmas and suffer from insufficient spectral resolution or contamination from overlapping satellite transitions.

In this Letter, we present detailed x-ray line shape measurements of He β emitted from thin-slab Ti plasmas near solid density. The line shapes were observed with high spectral resolution ($E/\Delta E \sim 10^4$), with statistical error quantified by repeated measurements and plasma gradients minimized via emission localization in a thin tracer layer. When tracer layers move deeper relative to the laser-heated target surface, He β line shapes shift, broaden, and split into two apparent peaks. The suite of measurements is analyzed with a Markov chain Monte Carlo (MCMC) framework, used to estimate probability distributions of plasma density and temperatures by comparing data to two line shape theory approximations. The first calculation [21] employs the dipole approximation for the interaction between free and bound electrons, and subsequently cannot model dense plasma redshifts, leaving an unresolved ambiguity between ion temperature T_i and electron density n_e . While dependence of Stark broadening on T_i is well-known [22–25], this general ambiguity versus n_e has gone largely unacknowledged in the literature. A second theory model [17,26,27] treats collisions as full Coulomb interactions; including the monopole term enables prediction of dense plasma redshifts, which depend differently on n_e and T_i than the

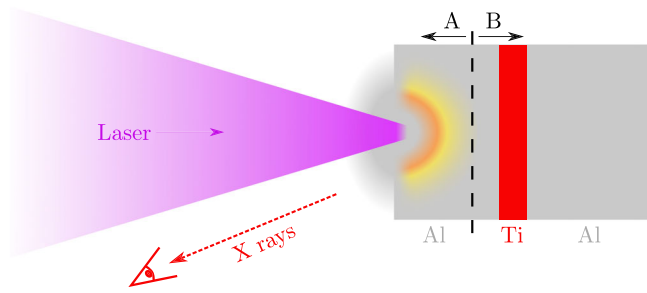


FIG. 1. A not-to-scale cartoon schematic of the experimental setup, including the normally incident laser pulse, the Al target with an embedded Ti layer, and the viewing angle of the x-ray spectrometer. Two target regions are shown: the dynamic shallow region (A) and the stationary deep region (B).

broadening alone. Redshifts thus produce a new fitting constraint that resolves the ambiguity. Crucially, these improvements in both measurement and calculation constrain not only near-solid-density n_e , but also T_i and electron temperature T_e . This final capability provides strong experimental evidence that ions and electrons are *not* in thermal equilibrium in this laser-heated, solid-density system, despite theoretically short thermalization times. Our simultaneous local measurements of T_i and T_e in high-density plasmas with minimized spatial gradients are therefore of interest for studying ion-electron equilibration.

Observations were made at the ALEPH 400 nm [28], a laser with 8–10 J pulses of duration 45 fs; focal spots of radius $\lesssim 1.5 \mu\text{m}$ produce relativistic intensities above $3 \times 10^{21} \text{ W/cm}^2$. Ultrahigh temporal contrast ($> 10^{12}$ at 25 ps) prevents solid laser targets from expanding early due to prepulse laser light. In these conditions, laser pulses heat targets via ion shocks [29] and Ohmic return currents induced by laser-driven relativistic electrons [30], though the latter is expected to be more relevant for the deeply buried plasmas studied here. The illuminated targets were Al foils of thickness 20–25 μm with embedded Ti tracer layers of thickness 125 nm, with the laser normally incident as depicted in Fig. 1. A suite of target configurations was constructed by burying tracer layers under Al tamper layers of thickness 0–2.5 μm , thus placing the tracer at various depths z_{Ti} with respect to the laser-facing surface. The high repetition rate of the laser allowed 10 independent shots to build statistics for each target configuration; shot-to-shot variation in intensity is encapsulated in the figures by shaded areas. Each interaction was observed 22.5° from target normal by an x-ray-diffracting Bragg crystal spectrometer. The time-integrating setup, thoroughly described elsewhere [31], focuses x rays on a charge-coupled device detector with high spectral resolution so that all spectral features are effectively broadened only by plasma gradients (minimized via thin tracer layers) and plasma broadening effects. The entire spectrometer assembly was fixed in space, so all measurements shown herein have the same

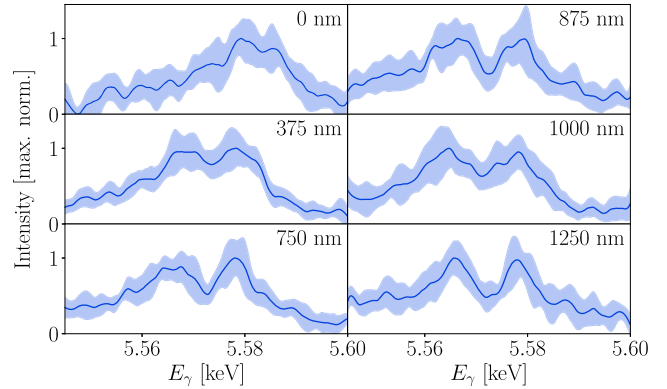


FIG. 2. Ti He β as a function of z_{Ti} as labeled (lines, 10-shot means; shaded regions, standard deviations). A nonperturbative Savitzky-Golay filter with span 3 eV has been applied.

spectral dispersion. The total uncertainty in the dispersion, given the observed length of the x-ray focus and known engineering tolerances, is $\sim \pm 3\%$.

Ti He β line shapes sampled from a variety of depths z_{Ti} are shown in Fig. 2. Thin tracer layers yield a relatively weak signal, giving an overall signal-to-noise ratio (SNR) of approximately 5. Nonetheless, several features of the line shapes are immediately evident: lines broaden and shift to lower energies with increasing z_{Ti} —a simplistic analysis of these qualities is examined in the Supplemental Material [32]—and for deeper z_{Ti} a dip is clearly present. This double-peaked structure is a hallmark of He β Stark broadening, with mixed energy levels $1s3\ell$ separating into two primary clusters as plasma microfields strengthen. Two peaks are not obviously evident from shallow layers, i.e., from the dynamic region A shown in Fig. 1 where plasma expansion, corresponding Doppler shifts, and spatiotemporal gradients are significant; however, dips are apparent in spectra from the deeper Region B ($z_{\text{Ti}} \gtrsim 750 \text{ nm}$), where measurements are approximately constant with depth. We focus this work on spectra from the more quiescent Region B. The dip between peaks was sought in previous experiments but was obscured by ion dynamics, mitigated here by the absence of low mass ions, and possibly also by spatial gradients [33]. In our case, the ultrathin Ti region significantly limits axial gradients, whereas radial and temporal gradients are present but de-emphasized by the strong weighting of He-like x-ray emission with higher n_e and T_e . The resulting observations can therefore inform on x-ray-weighted plasma parameters, which influence Stark line shapes and can thus be inferred from characteristics such as peak separation, line width, and redshift [20,34].

Even with poor SNR, peak fitting remains a viable strategy for accurately locating spectral features like the He β double peak, since reducing many intensity points to a single peak centroid enhances precision despite noise [35,36]. A seven-parameter fitting model was thus constructed that consisted of two summed Voigt functions,

each with a mean energy E_0 . The “best-fit” model parameters for each observation were inferred with an ensemble MCMC algorithm EMCEE [37], which is well suited to finding the distribution of Voigt-model inputs consistent with the data and its shot-to-shot variance. The converged [38] results contain a distribution of peak separations $\Delta E = E_{0,2} - E_{0,1}$; for example, at $z_{\text{Ti}} = 875$ nm, 80% of the samples are within $\Delta E = 13.0_{-0.6}^{+0.7}$ eV.

To connect this observed peak separation with physically meaningful insight, theoretical Stark-broadened line shapes for given plasma conditions must be calculated and their corresponding peak separations tabulated. This process is not trivial: the Stark mixing and shifting of each $1s3\ell$ state must be established as a function of the electric field, which relies on detailed atomic physics; and plasma microfields must be estimated and averaged, incorporating contributions from ions and electrons. Simplified formulas have been employed as approximations [1,20,39,40], but the full procedure requires dedicated line shape theory. We begin here by considering MERL [21], a broadly used line shape code that inputs ion microfield distributions from APEX [41] and treats all collisions as dipole interactions.

A series of MERL line shapes were computed and their maxima located, thereby calculating ΔE on a grid of varied T_i and n_e as mapped in Fig. 3(a). The electron temperature T_e was found to have little impact on the double-peak structure: since ions are essentially stationary over line emission timescales, only they create the quasistatic electric fields that maintain strong Stark shifts over time, while electrons do not produce sustained fields. The results show ΔE increasing with both n_e and T_i , which is reasonable

given that ion microfields correlate with both parameters. At higher n_e , ions pack more tightly near the emitter and strengthen the microfield; at higher T_i , faster ions more easily overcome ion-ion repulsion, leading to closer approaches and higher field values. This dual dependence, however, means that constraining plasma parameters based on peak separation is ill posed, with multiple values of n_e and T_i valid for each ΔE . The continuous band in the figure, showing the region within the experimental error bar, reflects this ambiguity.

Certainly, a complete line shape calculation constrains line shapes more fully than ΔE alone. In the hope of constraining both n_e and T_i , another MCMC search was performed, now comparing data to the entire MERL line shape from a new five-parameter model that includes n_e , T_i , and T_e . This approach necessitates inclusion of Li-like satellites to He β , which arise from similar $3 \rightarrow 1$ transitions but with a spectator electron in $n = 2, 3$, or 4 that modifies the transition energy. The ratio of each set of satellites ($n = 2, 3$, or 4) to the main line was determined by population ratios in the collisional-radiative code CRETIN [42] using atomic data calculated in FAC [43]. (Line ratios are practically identical to independent calculations from a similar code SCRAM [44].) A collection of resulting synthetic spectra is overlaid with fitted data in Fig. 3(b).

Even this full approach, including satellite structure and electron broadening, is unable to resolve the $n_e - T_i$ ambiguity. Shown in Fig. 3(c) is the converged likelihood probability, flattened in the $n_e \times T_i$ plane. A similar band as in Fig. 3(a) appears, with three main differences. Firstly, since the algorithm enforced $T_i \leq T_e$ (as expected in short-pulse-heated solids), the band cuts off above $T_i \sim 1$ keV. Secondly, the probability is clustered near the low- T_i boundary, necessarily included due to numerical issues at low T_i/T_e . This clustering is a byproduct of the ensemble MCMC algorithm, where random walkers attempt to explore probable but disallowed regions (plotted MERL line shapes oversample regions at low density to showcase the uniformity of results throughout the band). Lastly, the band occurs at noticeably lower n_e and T_i than before; note in Fig. 3(b) that the modeled line shapes prioritize line wings and dip narrowness, placing peaks marginally closer together than they appear in the data. Importantly, the search does indicate an unambiguous $T_e = 1080_{-90}^{+130}$ eV, with the full distribution shown in Fig. 3(d); this determination is a result of well-constrained satellites (both $n = 2$ and $n = 3$) that would be too intense at lower temperatures. Note that full line shape fitting, especially the T_e derivation, is influenced by small but non-negligible opacity, since radiation transport modifies relative intensities; as such, a peak optical depth $\tau = 0.2$, as estimated by CRETIN, is included in both this model and the second line shape model below. Nevertheless, since T_e is derived solely through the intensity of Li-like satellites and has minimal impact on the double-peak structure, constraining it does

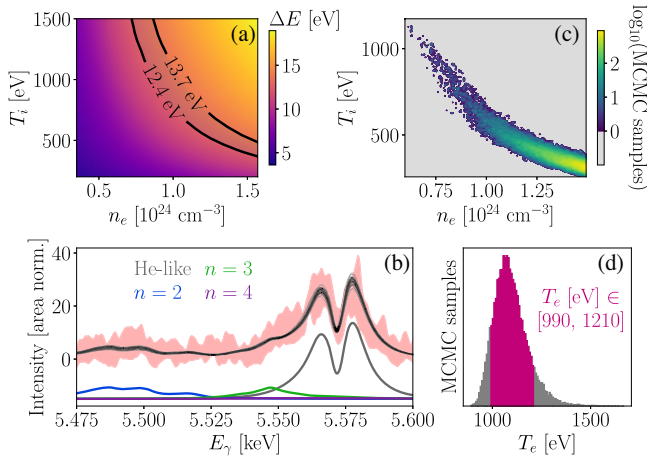


FIG. 3. For $z_{\text{Ti}} = 875$ nm: (a) A colormap of ΔE from MERL versus n_e and T_i , with a band showing measured values. (b) Calculated MERL line shapes, including satellites, sampled from the EMCEE-calculated likelihood distribution (black) overlaying the data (shaded red). Example satellite contributions are vertically offset. (c) Estimated likelihood map for full MERL fits over a similar space to (a). (d) Histogram of T_e values from the same MCMC search, with middle 80% highlighted.

not resolve the $n_e - T_i$ ambiguity that manifests again here. (Neither improving SNR via thicker tracer layers nor including $1s4\ell$ states in Stark line shape mixing changed these conclusions.)

The Stark-broadened line shapes calculated with MERL employed a dipole interaction approximation for the electron broadening [21]. Though widespread and computationally inexpensive, this approximation neglects the full Coulomb interaction that accounts for both line broadening and redshifts [16], as was included in alternative versions of MERL [9,17]. Thus a more comprehensive Stark broadening code, BALROG, was consulted for fitting to the data. BALROG is an analytic, quantum-mechanical line shape calculator that does not truncate terms from the Coulomb potential, thereby accounting for electron penetration into ionic orbitals as is important for highly charged ions like Ti^{20+} [26,27]. Because this model includes monopole terms that shift all transitions uniformly, it has the capability to model redshifts as well as line broadening and peak separation.

For the purpose of fitting this second line shape theory to the data, a grid of BALROG line shapes was obtained for various n_e and T_i , assuming $T_e = 1$ keV from the aforementioned line ratios; each calculation is seen to redshift relative to the calculated energy of $\text{He}\beta$ at low density. These line shapes are linearly interpolated for computational tractability to produce spectra at continuous values of $n_e \in [6, 14] \times 10^{23} \text{ cm}^{-3}$ and $T_i \in [400, 1000] \text{ eV}$. These calculations are directly comparable to measurements, provided that the data is referenced to an experimental “unshifted” line position. Here, we take the maximum of the untamped ($z_{\text{Ti}} = 0$) line shape as an approximate reference energy; since this measured location may still be shifted due to Doppler and/or Stark effects, an uncertainty in overall redshift of ± 2 eV is included in the fitting and reflected in the following error analysis.

A distribution of BALROG line shapes consistent with the data are obtained with the same MCMC framework described above and depicted in Fig. 4(a). Now that the measured spectra are referenced to calculations from a full Coulomb line shape theory that includes redshifts, the local plasma parameters are tightly constrained, with likelihood distribution shown in Fig. 4(b) and 80% confidence intervals $n_e \in [1.0, 1.3] \times 10^{24} \text{ cm}^{-3}$ and $T_i \in [530, 690] \text{ eV}$. The analysis was independently repeated on data from $z_{\text{Ti}} = 750, 875, 1000,$ and 1250 nm , all of which maximize likelihood at $n_e > 10^{24} \text{ cm}^{-3}$ and $T_i < 750 \text{ eV}$; this consistency further evidences the homogeneity of the tamped plasma. (An analysis method that compares only the measured peak centroids to BALROG, akin to the peak separation analysis in Fig. 3(a), is qualitatively consistent with the above and described in the Supplemental Material [32].) The line shape fits indicate that a well-tamped region reaches $T_e \sim 1$ keV while maintaining densities over 80% of solid ($n_e^{\text{solid}} = 1.2 \times 10^{24} \text{ cm}^{-3}$ in He-like Ti).

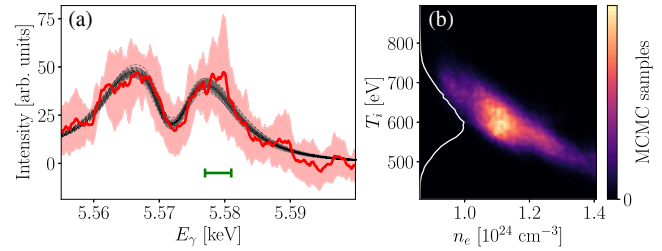


FIG. 4. (a) Comparison between redshifted data from $z_{\text{Ti}} = 875 \text{ nm}$ (red line and shaded error bar) and BALROG line shapes from the distribution of fits (dashed black). The reference energy is free to vary in the MCMC fitting within the range of the green error bar. (b) The corresponding likelihood distribution of (n_e, T_i) values, with histogram of T_i only shown on the left.

The ability of short-pulse, high-contrast lasers to heat demonstrably solid-density material to high temperatures is of interest for collision-based high-energy-density plasma experiments and for benchmarking models that have particular challenges in this regime.

Moreover, this analysis strongly suggests ($> 99.9\%$ probability given the distributions shown) that ions are unequibrated with electrons, with $T_i < T_e$, for all z_{Ti} between 750 nm and $1.25 \mu\text{m}$; a systematic error of 20% in T_e would still refute equilibration with $> 99\%$ probability. Since both T_e and T_i are derived from x rays of the same energy ($\sim 5.5 \text{ keV}$), both measurements emphasize the same hot plasma region and therefore support the coexistence of warmer electrons and cooler ions. This conclusion is unexpected, given an ion-electron thermal equilibration time from Spitzer, $\nu_{ie}^{-1} \sim 0.5 \text{ ps}$ [45], much shorter than the duration of x-ray emission $\sim 5 \text{ ps}$ (as inferred from similar experiments with Ni at ALEPH [46]). The temperature difference survives time integration: it is reflective of the average $\text{He}\beta$ -emitting plasma and is thus not transient. As such, either (i) equilibration is slower than Spitzer predicts or (ii) there exists a surprisingly strong channel of ion energy loss. Concerning the former, many modifiers of thermalization, including degeneracy and instabilities, would shorten equilibration times, but some theories and experiments in warm dense conditions have also seen anomalously long equilibration times [47,48]. Though such systems are substantially more coupled than the much hotter plasma examined here, our lack of equilibration seems consistent with this previous work. As for the latter possibility, ions do not cool via radiation but may from thermal conduction to nearby cold material. Classical, unmagnetized ion heat transport [49] is far too slow to balance thermalization with realistic gradient length scales $\sim 1 \mu\text{m}$, but anomalous heat transport, driven perhaps by turbulence, may provide the necessary cooling. Given the ubiquity of assuming $T_i = T_e$ based on short thermal equilibration times, and the scarcity of dense systems where simultaneous measurements of T_i and T_e are currently possible [50], our inference of unequibrated

ions warrants further exploration in both theory and experiment. Notably, the present platform, where well-tamped plasmas with minimal spatial gradients are comprehensively diagnosed via high-resolution He β line shapes, may be suitable for more detailed studies of ion-electron equilibration in dense plasmas; for example, experimental development may enable time-resolving He β line shapes with streak cameras, deepening insight into the plasma power balance.

The line shape analysis presented here has successfully determined plasma parameters n_e , T_e , and T_i from the Ti He β Stark-broadened line shape including overall redshift. We highlight a central ambiguity in relying on line widths or peak separation alone, which cannot constrain n_e and T_i without further input. We believe this difficulty is usually underappreciated in Stark broadening analysis: unless n_e or T_i is explicitly limited by extra information [25], the plasma conditions cannot be determined solely by Stark width or line shape. Here, we constrain both parameters by accounting for dense plasma redshifts, which arise from monopole Coulomb interactions and are therefore excluded in the standard Stark broadening theory approximation of dipole interaction for electron broadening. Since redshifts exhibit different dependence on n_e and T_i than peak separations, this new constraint resolves the fitting ambiguity. Our study is the first to couple advanced line shape models including redshift with detailed, high-resolution line shape measurements showing distinct peak features. It is also the first to invalidate the assumed thermalization of ions with electrons in solid-density plasmas. Our technique may be broadly applicable for diagnosing hot plasmas near solid density.

The authors acknowledge the helpful calculations and insight of S. B. Hansen. This work was supported by the DOE Office of Science, Fusion Energy Sciences under Contract No. DE-SC0021246: the LaserNetUS initiative at Colorado State University's Advanced Beam Laboratory, and was performed under the auspices of the U.S. Department of Energy by Princeton Plasma Physics Laboratory under Contract No. DE-AC02-09CH11466 and by Lawrence Livermore National Laboratory under Contract No. DE-AC52-07NA27344. The work of T. A. Gomez was performed under the Laboratory Directed Research and Development program at Sandia National Laboratories, a multimission laboratory managed and operated by National Technology & Engineering Solutions of Sandia, LLC, a wholly owned subsidiary of Honeywell International Inc., for the U.S. Department of Energy's National Nuclear Security Administration under Contract No. DE-NA0003525. This paper describes objective technical results and analysis. Any subjective views or opinions that might be expressed in the paper do not necessarily represent the views of the U.S. Department of Energy or the United States Government.

*Corresponding author.

bkraus@pppl.gov

- [1] M. Baranger, General impact theory of pressure broadening, *Phys. Rev.* **112**, 855 (1958).
- [2] H. Griem, *Spectral Line Broadening by Plasmas* (Elsevier, New York, 2012).
- [3] P.-E. Tremblay and P. Bergeron, Spectroscopic analysis of DA white dwarfs: Stark broadening of hydrogen lines including nonideal effects, *Astrophys. J.* **696**, 1755 (2009).
- [4] R. E. Falcon, G. A. Rochau, J. E. Bailey, T. A. Gomez, M. H. Montgomery, D. E. Winget, and T. Nagayama, Laboratory measurements of white dwarf photospheric spectral lines: H β , *Astrophys. J.* **806**, 214 (2015).
- [5] T. A. Gomez, T. Nagayama, D. P. Kilcrease, M. H. Montgomery, and D. E. Winget, Effect of higher-order multipole moments on the Stark line shape, *Phys. Rev. A* **94**, 022501 (2016).
- [6] F. Paerels, Pressure broadening of absorption lines in neutron star atmospheres and prospects for measuring neutron star masses and radii, *Astrophys. J. Lett.* **476**, L47 (1997).
- [7] M. S. Dimitrijević, Stark broadening in astrophysics (applications of Belgrade school results and collaboration with former Soviet Republics), *Astronomical and Astrophysical Transactions* **22**, 389 (2003).
- [8] R. Lee, Effect of fine-structure splitting on the shape of the Lyman α line profile of high- z emitters in ultra dense plasmas, *Phys. Lett. A* **71**, 224 (1979).
- [9] A. Saemann, K. Eidmann, I. E. Golovkin, R. C. Mancini, E. Andersson, E. Förster, and K. Witte, Isochoric Heating of Solid Aluminum by Ultrashort Laser Pulses Focused on a Tamped Target, *Phys. Rev. Lett.* **82**, 4843 (1999).
- [10] E. Stambulchik and Y. Maron, Plasma line broadening and computer simulations: A mini-review, *High Energy Density Phys.* **6**, 9 (2010).
- [11] M. A. Gigosos, Stark broadening models for plasma diagnostics, *J. Phys. D* **47**, 343001 (2014).
- [12] P. Beiersdorfer, G. V. Brown, A. McKelvey, R. Shepherd, D. J. Hoarty, C. R. D. Brown, M. P. Hill, L. M. R. Hobbs, S. F. James, J. Morton *et al.*, High-resolution measurements of Cl¹⁵⁺ line shifts in hot, solid-density plasmas, *Phys. Rev. A* **100**, 012511 (2019).
- [13] N. C. Woolsey, B. A. Hammel, C. J. Keane, A. Asfaw, C. A. Back, J. C. Moreno, J. K. Nash, A. Calisti, C. Mossé, R. Stamm *et al.*, Evolution of electron temperature and electron density in indirectly driven spherical implosions, *Phys. Rev. E* **56**, 2314 (1997).
- [14] I. Golovkin, R. Mancini, S. Louis, Y. Ochi, K. Fujita, H. Nishimura, H. Shirga, N. Miyanaga, H. Azechi, R. Butzbach *et al.*, Spectroscopic Determination of Dynamic Plasma Gradients in Implosion Cores, *Phys. Rev. Lett.* **88**, 045002 (2002).
- [15] H. Chen, T. Ma, R. Nora, M. Barrios, H. Scott, M. Schneider, L. Berzak Hopkins, D. Casey, B. Hammel, L. Jarrott *et al.*, On krypton-doped capsule implosion experiments at the National Ignition Facility, *Phys. Plasmas* **24**, 072715 (2017).
- [16] H. Nguyen, M. Koenig, D. Benredjem, M. Caby, and G. Coulaud, Atomic structure and polarization line shift in dense and hot plasmas, *Phys. Rev. A* **33**, 1279 (1986).

- [17] G. C. Junkel, M. A. Gunderson, C. F. Hooper, Jr., and D. A. Haynes, Jr., Full Coulomb calculation of Stark broadened spectra from multielectron ions: A focus on the dense plasma line shift, *Phys. Rev. E* **62**, 5584 (2000).
- [18] R. Mancini, C. Iglesias, S. Ferri, A. Calisti, and R. Florido, The effect of improved satellite line shapes on the argon He β spectral feature, *High Energy Density Phys.* **9**, 731 (2013).
- [19] S. Ferri, A. Calisti, C. Mossé, J. Rosato, B. Talin, S. Alexiou, M. A. Gigosos, M. A. González, D. González-Herrero, N. Lara *et al.*, Ion dynamics effect on Stark-broadened line shapes: A cross-comparison of various models, *Atoms* **2**, 299 (2014).
- [20] M. F. Gu and P. Beiersdorfer, Stark shift and width of x-ray lines from highly charged ions in dense plasmas, *Phys. Rev. A* **101**, 032501 (2020).
- [21] R. Mancini, D. Kilcrease, L. Woltz, and C. Hooper, Jr., Computational aspects of the Stark line broadening of multi-electron ions in plasmas, *Comput. Phys. Commun.* **63**, 314 (1991).
- [22] R. J. Tighe and C. F. Hooper, Jr., Low-frequency electric microfield distributions in a plasma containing multiply-charged ions: Extended calculations, *Phys. Rev. A* **15**, 1773 (1977).
- [23] C. Iglesias, F. Rogers, R. Shepherd, A. Bar-Shalom, M. Murillo, D. Kilcrease, A. Calisti, and R. Lee, Fast electric microfield distribution calculations in extreme matter conditions, *J. Quant. Spectrosc. Radiat. Transfer* **65**, 303 (2000).
- [24] K. B. Fournier, B. Young, S. Moon, M. Foord, D. Price, R. Shepherd, and P. Springer, Characterization of time resolved, buried layer plasmas produced by ultrashort laser pulses, *J. Quant. Spectrosc. Radiat. Transfer* **71**, 339 (2001).
- [25] D. Alumot, E. Kroupp, E. Stambulchik, A. Starobinets, I. Uschmann, and Y. Maron, Determination of the Ion Temperature in a High-Energy-Density Plasma Using the Stark Effect, *Phys. Rev. Lett.* **122**, 095001 (2019).
- [26] T. Gomez, Spectral line broadening: Radiator-plasma interactions, Technical Report, Sandia National Lab.(SNL-NM), Albuquerque, NM, USA, 2017.
- [27] T. Gomez, T. Nagayama, P. Cho, M. Zammit, C. Fontes, D. Kilcrease, I. Bray, I. Hubeny, S. Hansen, B. Dunlap, M. Montgomery, and D. Winget, All-Order Full-Coulomb Quantum Line-Shape Calculations, *Phys. Rev. Lett.* (to be published).
- [28] Y. Wang, S. Wang, A. Rockwood, B. M. Luther, R. Hollinger, A. Curtis, C. Calvi, C. S. Menoni, and J. J. Rocca, 0.85 PW laser operation at 3.3 Hz and high-contrast ultrahigh-intensity $\lambda = 400$ nm second-harmonic beamline, *Opt. Lett.* **42**, 3828 (2017).
- [29] K. U. Akli, S. B. Hansen, A. J. Kemp, R. R. Freeman, F. N. Beg, D. C. Clark, S. D. Chen, D. Hey, S. P. Hatchett, K. Highbarger *et al.*, Laser Heating of Solid Matter by Light-Pressure-Driven Shocks at Ultrarelativistic Intensities, *Phys. Rev. Lett.* **100**, 165002 (2008).
- [30] C. R. D. Brown, D. J. Hoarty, S. F. James, D. Swatton, S. J. Hughes, J. W. Morton, T. M. Guylmer, M. P. Hill, D. A. Chapman, J. E. Andrew *et al.*, Measurements of Electron Transport in Foils Irradiated with a Picosecond Time Scale Laser Pulse, *Phys. Rev. Lett.* **106**, 185003 (2011).
- [31] B. Kraus, A. Chien, L. Gao, K. Hill, M. Bitter, P. Efthimion, H. Chen, M. Schneider, A. Moreau, R. Hollinger *et al.*, Comparing plasma conditions in short-pulse-heated foils via fine-structure x-ray emission, *Rev. Sci. Instrum.* **92**, 033525 (2021).
- [32] See Supplemental Material at <http://link.aps.org/supplemental/10.1103/PhysRevLett.127.205001> for two secondary analyses of the data.
- [33] D. A. Haynes, Jr., D. T. Garber, C. F. Hooper, Jr., R. C. Mancini, Y. T. Lee, D. K. Bradley, J. Delettrez, R. Epstein, and P. A. Jaanimagi, Effects of ion dynamics and opacity on Stark-broadened argon line profiles, *Phys. Rev. E* **53**, 1042 (1996).
- [34] X. Li, F. Rosmej, V. Lisitsa, and V. Astapenko, An analytical plasma screening potential based on the self-consistent-field ion-sphere model, *Phys. Plasmas* **26**, 033301 (2019).
- [35] O. Renner, P. Adámek, P. Angelo, E. Dalimier, E. Förster, E. Krousky, F. Rosmej, and R. Schott, Spectral line decomposition and frequency shifts in Al He α group emission from laser-produced plasma, *J. Quant. Spectrosc. Radiat. Transfer* **99**, 523 (2006).
- [36] F. Khattak, O. P. du Sert, F. Rosmej, and D. Riley, Evidence of plasma polarization shift of Ti He- α resonance line in high density laser produced plasmas, *J. Phys. Conf. Ser.* **397**, 012020 (2012).
- [37] D. Foreman-Mackey, D. W. Hogg, D. Lang, and J. Goodman, emcee: The MCMC Hammer, *Publ. Astron. Soc. Pac.* **125**, 306 (2013).
- [38] J. Goodman and J. Weare, Ensemble samplers with affine invariance, *Commun. Appl. Math. Comput. Sci.* **5**, 65 (2010); All EMCEE output in this work has integrated autocorrelation times $\gg 100$.
- [39] A. Y. Potekhin, G. Chabrier, and D. Gilles, Electric microfield distributions in electron-ion plasmas, *Phys. Rev. E* **65**, 036412 (2002).
- [40] E. Stambulchik and Y. Maron, Stark effect of high-n hydrogen-like transitions: quasi-contiguous approximation, *J. Phys. B* **41**, 095703 (2008).
- [41] C. A. Iglesias, H. E. DeWitt, J. L. Lebowitz, D. MacGowan, and W. B. Hubbard, Low-frequency electric microfield distributions in plasmas, *Phys. Rev. A* **31**, 1698 (1985).
- [42] H. A. Scott, Cretin—a radiative transfer capability for laboratory plasmas, *J. Quant. Spectrosc. Radiat. Transfer* **71**, 689 (2001).
- [43] M. F. Gu, The flexible atomic code, *Can. J. Phys.* **86**, 675 (2008).
- [44] S. Hansen, J. Bauche, C. Bauche-Arnoult, and M. Gu, Hybrid atomic models for spectroscopic plasma diagnostics, *High Energy Density Phys.* **3**, 109 (2007).
- [45] H. Brysk, Electron-ion equilibration in a partially degenerate plasma, *Plasma Phys.* **16**, 927 (1974).
- [46] R. Hollinger (to be published).
- [47] M. W. C. Dharma-Wardana and F. Perrot, Energy relaxation and the quasiequation of state of a dense two-temperature nonequilibrium plasma, *Phys. Rev. E* **58**, 3705 (1998).
- [48] T. G. White, N. J. Hartley, B. Borm, B. J. B. Crowley, J. W. O. Harris, D. C. Hochhaus, T. Kaempfer, K. Li, P. Neumayer, L. K. Pattison *et al.*, Electron-Ion Equilibration in Ultrafast Heated Graphite, *Phys. Rev. Lett.* **112**, 145005 (2014).

- [49] S. Braginskii, Transport phenomena in a completely ionized two-temperature plasma, *Sov. Phys. JETP* **6**, 358 (1958).
- [50] H. Sio, J. Frenje, J. Katz, C. Stoeckl, D. Weiner, M. Bedzyk, V. Glebov, C. Sorce, M. Gatu Johnson, H. Rinderknecht *et al.*, A particle x-ray temporal diagnostic (PXTD) for studies of kinetic, multi-ion effects, and ion-electron equilibration rates in inertial confinement fusion plasmas at OMEGA (invited), *Rev. Sci. Instrum.* **87**, 11D701 (2016).